AUTOMATIC DETECTION OF UNMINEABLE INCLUSIONS WHILE BUCKET WHEEL EXCAVATOR DIGGING, USING ELECTROMAGNETIC (EM) SENSOR AND GPS

OUTOMATYCZNE WYKRYWANIE WTRĄCEŃ NIEURABIALNYCH PODCZAS URABIANIA KOPARKĄ WIELOCZERPAKOWĄ KOŁOWĄ PRZY UŻYCIU CZUJNIKA ELEKTROMAGNETYCZNEGO (EM) I GPS

Michael Galetakis, Antonios Vafidis, George Kritikakis, Vasileios Deligiorgis - Technical University of Crete, Greece
Theodore Michalakopoulos, George Apostolopoulos - National Technical University of Athens, Greece
Christos Roumpos, Fragkiskos Pavloudakis - Public Power Corporation SA, Greece

This work describes a methodology for the automatic detection of unmineable inclusions while bucket wheel excavator (BWE) digging, using electromagnetic (EM) sensor and GPS. The overall methodology consists of data collection, pre-processing and evaluation. Two different data evaluation approaches were developed and implemented in Matlab programming environment. A relatively simple one called Simple Mode, based on statistical process control and a more sophisticated one, called Advanced Mode, based on Position Prominence Index (PPI) and on Neural-Network based Pattern Recognition (NNPR). Synthetic electromagnetic data created and used (both in simple and advanced mode) for testing the algorithms extensively. Real data, surveyed by moving the EM sensor (CMD2 of GF Instruments) and GPS against a mine slope, were examined with the proposed methodology as well. Advanced Mode provided more accurate results than Simple Mode in automatic detection of unmineable inclusions. However it is sensitive in positioning accuracy and it requires access to EM data acquired in successive bucket wheel cuts.

Keywords: *bucket wheel excavator, unmineable inclusions detection, electromagnetic geophysical methods, automated algorithm*

W pracy opisano metodologię automatycznego wykrywania nieurabialnych wtrąceń podczas normalnej pracy koparki wielonaczyniowej (BWE) przy użyciu czujnika elektromagnetycznego (EM) i GPS. Ogólna metodologia obejmuje gromadzenie danych, wstępne przetwarzanie oraz ocenę. Opracowano dwa różne warianty oceny danych i wdrożono je w środowisku programowania Matlab. Stosunkowo prosty, zwany Simple Mode, oparty na statystycznej kontroli procesu i bardziej zaawansowany, zwany Advanced Mode, oparty na Position Prominence Index (PPI) oraz na Neural-Network based Pattern Recognition (NNPR). Utworzono i wykorzystano syntetyczne dane elektromagnetyczne (zarówno w trybie prostym, jak i zaawansowanym) do wszechstronnego testowania algorytmów. Uzyskane w warunkach terenowych dane pochodzące z czujnika EM (CMD2 z GF Instruments) i GPS przesuwanych na skarpie zabierki, zostały również przeanalizowano przy zastosowaniu ww. metodologii. Tryb zaawansowany (Advanced Mode) zapewnia dokładniejsze wyniki niż tryb prosty (Simple Mode) w automatycznym wykrywaniu nieurabialnych inkluzji. Jest jednak wrażliwy na dokładność pozycjonowania i wymaga dostępu do danych czujnika elektromagnetycznego (EM) uzyskanych w kolejno wybieranych przez koparkę wielonaczyniową pasmach zabierki.

Słowa kluczowe: *koparka wielonaczyniowa, wtrącenia nieurabialne, elektromagnetyczne metody geofizyczne, automatyczny algorytm*

INTRODUCTION

One of the frequent problems, when mining coal deposits with continuous surface operations, is the presence of hard formations, namely cohesive materials of high mechanical strength in relation to the other materials of the series. Often it is difficult or impossible to excavate these hard inclusions with BWEs (Kavouridis et al., 2008, Huss, 2014, Nan et al., 2008). The existence of these hard rock formations with high cutting resistance result in stoppage, increased equipment wear, or even severe damage of the bucket wheel excavator (BWE), resulting to increased idle and break-down time, to increased energy consumption, to lower production rate and finally to increased mining cost. To prevent the BWEs from digging into the hard formations a clear forward warning for the presence of hard inclusions is required. An extensive comparison, ranking and evaluation via field testing of several geophysical methods identified that, in the typical geologic

environment of lignite mines employing BWEs, the electromagnetic methods (EM) are the most promising in detecting local features such boulders and hard layers (Overmeyer et al., 2007, Galetakis et al., 2016). Thus if a continuously working geophysical sensor mounted on the BWE could scan the slope few cuts ahead of the face and detect hard inclusions, digging into them could be avoided (Galetakis et al., 2016). Field tests of the electromagnetics geophysical method (using the CMD2 sensor of GF Instruments) mounted on the BWE proved its effectiveness in opencast mines for detection of the ground ahead of the excavation face.

In this paper we present automated algorithms which predict the probability of occurrence of a hard rock formation at a specific position based on data received from an electromagnetic geophysical sensor mounted on the BWE boom. This sensor measures continuously the electrical conductivity of the subsurface in the mine face. The probability of occurrence of a hard rock formation is used as input to an expert system which estimates the risk of collision (between excavating buckets and hard rock formation) and if necessary, generates alarms.

First the modeling with EM and the overall system for data collection, processing and evaluation is briefly presented. Then the developed algorithms for the automatic data evaluation are descripted and tested with synthetic and real data obtained from mine face geophysical survey. The obtained results are examined and the efficiency of the developed algorithms regarding their ability to predict the occurrence of hard rock formations during mining by BWEs is discussed.

MODELING ELECTROMAGNETIC DATA

The ground conductivity instruments use a phase sensitive measurement between the secondary (Hs) and the primary (Hp) magnetic fields. The instrument measurement involving the Hs/Hp is converted to apparent conductivity, with σ_a in S/m, using the formula:

$$\sigma_a = \frac{4}{\omega\mu_0 x^2}\frac{\mathrm{Im}(H_s)}{(H_p)} \qquad (1)$$

where ω is angular frequency, ω=2πf, f is the frequency in Hz, x is the Tx–Rx coil separation in m, μ_0 is the magnetic permeability of free space. Apparent resistivity is $\rho_a = 1/\sigma_a$ in Ohmm. This formula is valid if the induction number $B = x/\delta \ll 1$ where δ is the skin-depth.

A simple way of calculating the instrument reading on an arbitrary layered earth, as long as the intercoil spacing is much less that the skin depth in all of the layers, is to add the contribution of each layer independently, weighted according to its conductivity and thickness (McNeill, 1980).

In 2D approximation, a conductivity model is discretized in N (i=1,2,3,…,N) layers and M (j=1,2,3,…,M) blocks within each layer in z and x direction, respectively. Each discrete cell has a constant value of conductivity. Each cell has dimensions dz and dx in z and x direction, respectively. Here we propose a method for estimating apparent conductivities by adding the contribution of each cell independently, weighted according to its conductivity.

For coil separation of 1.89 m (which applies for the CMD2 instrument used in this study), low depth range mode and maximum depth of penetration 7 m, the cumulative sensitivity weighting factor is shown in Figure 1a. The corresponding synthetic apparent resistivity ($\rho_a = 1/\sigma_a$) profiles for both the 1D and 2D approaches are shown in Figure 1b, over a conductive half space containing two non-conductive bodies.

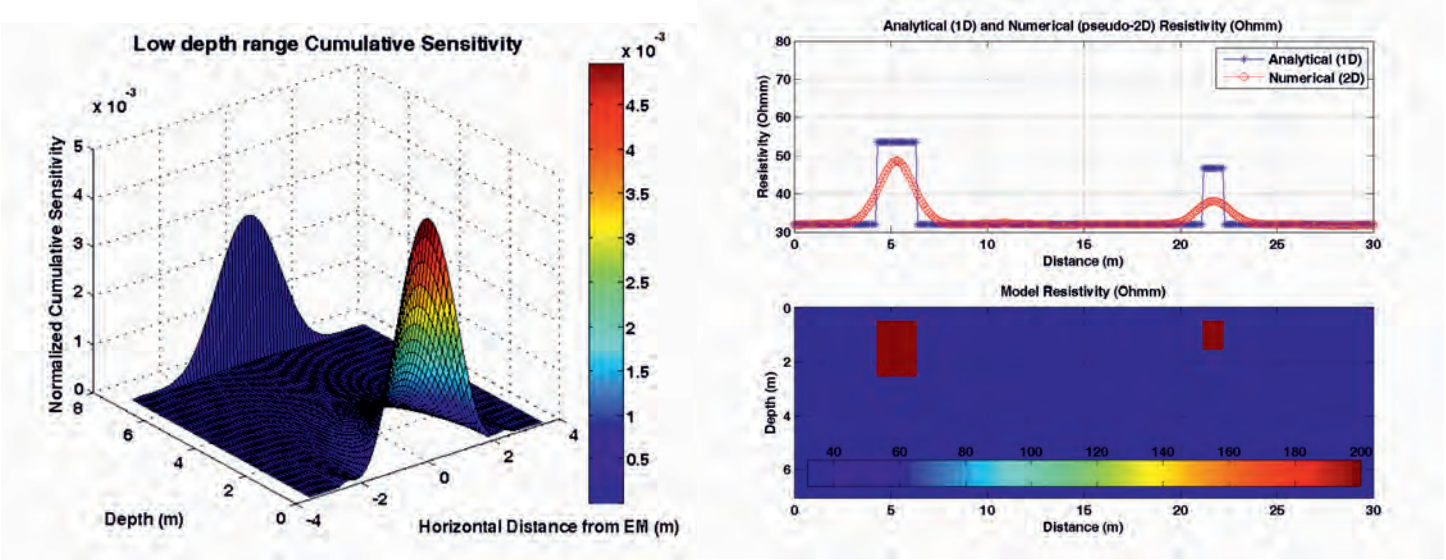

(a) (b)

Fig. 1. (a) Low depth range 2D normalized cumulative sensitivity for intercoil separation 1.89 m and maximum depth of penetration 7 m. The instrument is located at horizontal distance *x=0 m,* where maximum sensitivity values occur
(b) The synthetic apparent resistivity values over a 30 mx7 m model. Two resistive (200 Ohmm) bodies are buried at depth (top of bodies) 0.5 m from the surface within a homogeneous conductive (32 Ohmm) half space. These bodies generate characteristic high apparent resistivity anomalies.

Rys. 1. (a) Dwuwymiarowa znormalizowana czułość łączna niskiego zakresu głębokości dla separacji cewek 1,89 m i maksymalnej głębokości profilowania 7 m. Instrument znajduje się w odległości poziomej *x = 0 m,* gdzie występuje maksymalna czułość
. (b) Syntetyczne pozorne wartości rezystywności w modelu 30 mx7 m. Dwa ciała rezystancyjne (200 Ohmm) są zakopane na głębokości 0,5 m od powierzchni terenu w gruncie o jednorodnej przewodności (32 Ohmm). Ciała te generują charakterystyczne anomalie rezystywności

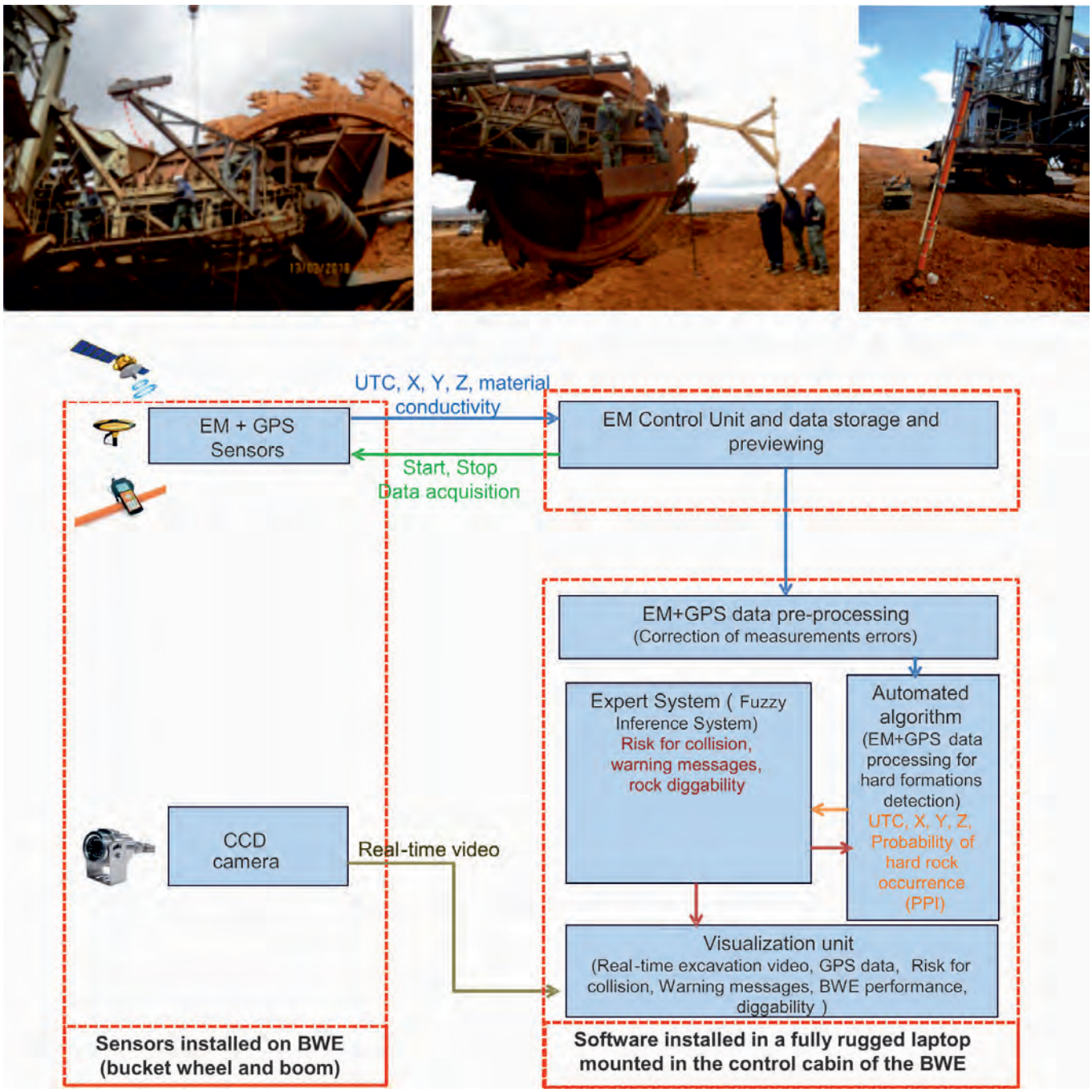

Fig. 2. Mounting of EM and GPS sensors on the bucket wheel boom (above) and block diagram of the measuring and processing system installed on the bucket wheel excavator (below)
Rys. 2. Montaż czujników EM i GPS na wysięgniku z kołem urabiającym (wyżej) oraz schemat blokowy układu pomiarowo-technologicznego zainstalowanego na koparce (niżej)

SYSTEM FOR DATA COLLECTION AND PROCESSING

The measuring and data processing system, as shown in Figure 2, consists of three subsystems. The first subsystem includes the measuring devices (EM sensor – CMD2, differential GPS and CCD camera) installed on the bucket wheel and the boom of BWE. The second subsystem is the EM control unit which collects, stores, transmits data and controls the operation of the EM sensor. GPS is connected and synchronized with EM sensor. Thus, the positioning and resistivity data from EM are transmitted simultaneously to control unit. The data, recorded in continuous mode at predefined sampling intervals, are: time (UTC, Coordinated Universal Time), coordinates (Latitude, Longitude, Altitude) and conductivity of the surveyed part of the mine face by the EM instrument. Finally, the third subsystem is the developed software, installed on a fully rugged laptop, hosted in the control cabin of the BWE, consisting of four modules. The first module receives data form EM control unit, performs the required pre-processing, and sends the corrected data to automated algorithm module. Automated algorithm module predicts the probability of occurrence of a hard rock formation at a specific position, and sends this information to expert system module. Expert system estimates the risk of collision (between excavating buckets and hard rock formation) and if necessary, generates alarms. The last module of the third subsystem is the visualization unit, which provides the machine operator with all required information

as well as with real-time video for the visual inspection of the mine-face. The automatic algorithm for data evaluation, which is crucial for the overall system performance, is presented in detail below.

ALGORITHMS FOR THE AUTOMATIC EVALUATION OF THE COLLECTED EM DATA

Existing methods for EM data evaluation are mainly based on conductivity data inversion which in our case can provide information about the size and location of hard rock inclusions based on the estimation of the conductivity spatial distribution ahead of the front. These inversion methods though, are currently utilized as a post processing technique, since they are computationally expensive and require the complete dataset along one or more profiles. Thus we concentrated to data-driven modeling and especially to statistical and to machine-learning methods. We have developed two different algorithms: a relatively simple one called Simple Mode, based on statistical process control and a more sophisticated one, called Advanced Mode, based on Position Prominence Index (PPI) and on Neural-Network based Pattern Recognition (NNPR).

dow containing 21 resistivity values to evaluate the Long Term Average (LTA) and standard deviation. A narrower moving data window containing 3 measurements is also used to check if the Short Term Average (STA) lies within pre-defined limits. In addition, the Short Term Average (STA) to Long Term Average (LTA) ratio is checked if it exceeds a pre-defined limit, as well. Based on the above mentioned criteria, an alarm indicator is issued if the STA exceeds both standard deviation and STA/LTA ratio limits. Figure 3 shows schematically how SMHRD works.

Figure 4a shows an example of SMHRD algorithm application on synthetic resistivity with 10% random added noise. The standard deviation and STA/LTA ratio limits are both set to 1.1. These best selected values were selected from performance evaluation. The above mentioned parameters resulted in 95% and 85% success rate on finding the boulders in last BW cut, when tested with 1 and 2 boulder models, respectively, while false alarms were 5% and 23%, respectively (Figure 4b). An alarm is considered successful if, at least one alarm position lies within the area of the shallowest hard rock horizontal extend, and false, if an alarm is issued in a position where no hard rock exists or it is located deeper. Since, the false alarms in the scenario of single boulder models is quite low (5%), the false alarm

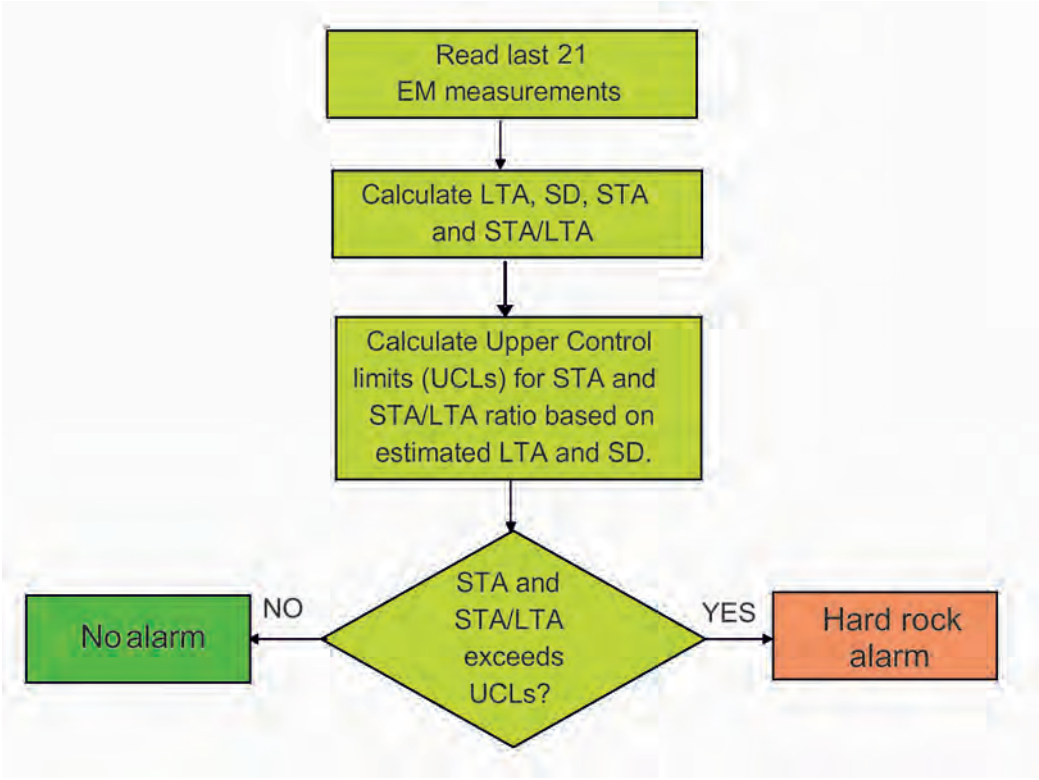

Fig. 3. Flowchart showing schematically the operation of Simple Mode algorithm used for the detection of hard rock formation during the operation of a BWE equipped with an EM geophysical sensor

Rys. 3. Schemat blokowy pokazujący zasadę działania algorytmu Simple Mode wykorzystywanego do wykrywania skał podczas urabiania koparką wielonaczyniową wyposażoną w czujnik geofizyczny EM

Simple Mode algorithm

The Simple Mode Hard Rock Detection (SMHRD) algorithm was developed to issue alarms when bucket wheel is approaching a hard rock formation. SMHRD is based on statistical process control and employs data collected during the current BWE cut. According to this approach, real-time CMD2 conductivity data are initially transformed to resistivity values and negative or extremely positive values are excluded (pre-processing). Then, SMHRD algorithm employs a moving average operator for a data win-

in the case of 2 boulder models is attributed to the detection of the deeper (and sometimes bigger) hard rock.

Another issue of SMHRD algorithm is the high success rate in deeper slice cuts (cut1-cut3 in Figure 4) than the current (cut4) resulting to early warning alerts. This is one of the most important reasons for the necessity of the development of more advanced techniques. Figure 5 shows a map of experimental apparent resistivity values acquired by moving CMD2 instrument mounted on a bucket truck against a slope, in June 2017 from South Field

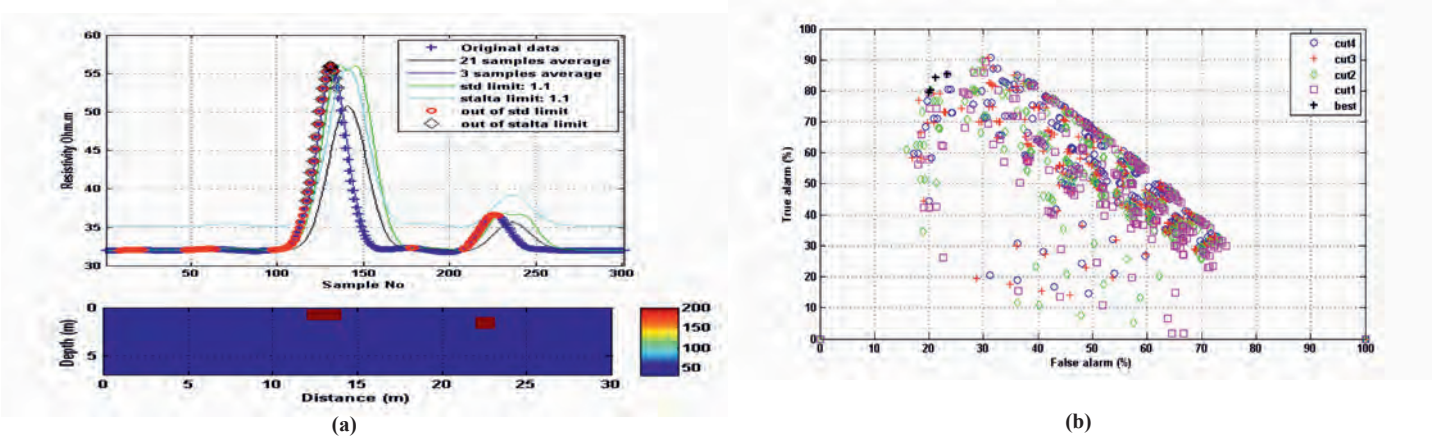

(a) (b)

Fig. 4: (a) Synthetic conductivity profile corresponding to the last BW cut before hitting the boulder, located at 0.2 m depth (the top of boulder) and 13 m (center) of model. The sampling interval in horizontal direction is 0.1 m and the color scale corresponds to resistivity in Ohmm. (b) Performance evaluation of SMHRD process for selected data windows and threshold limits, using synthetic resistivity data and successive BWE cuts. Cut4 correspond to the last BW cut before hitting on the boulder. Different BW cut depths (0.2, 0.6, 0.8, 1.0, 1.2 m) were examined in 100 different (randomly generated) 2 boulder models. The most successful parameter combinations, namely standard deviation and STA/LTA ratio limits, set to 1.1 and are highlighted with crosses

Rys. 4: (a) Syntetyczny profil przewodności odpowiadający wybieraniu ostatniego pasma przed uderzeniem koła wielonaczyniowego w kamień, znajdującego się na głębokości 0,2 m (górna krawędź wtrącenia skalnego) i na 13 m modelu (w środku). Przedział próbkowania w kierunku poziomym wynosi 0,1 m, a skala kolorów odpowiada rezystywności w Ohmm. (b) Ocena wydajności procesu SMHRD dla wybranych okien danych i wartości progowych, z wykorzystaniem syntetycznych danych rezystywności i kolejnych wybieranych pasm. Cut4 odpowiada ostatniemu wybranemu pasmu przed uderzeniem w głaz. Różne głębokości skrawania (0,2, 0,6, 0,8, 1,0, 1,2 m) zbadano w 100 różnych (losowo wygenerowanych) modelach z dwoma wtrąceniami. Najtrafniejsze kombinacje parametrów, odchylenie standardowe i limity współczynnika STA / LTA, ustawione na 1,1 i wyróżnione krzyżykami

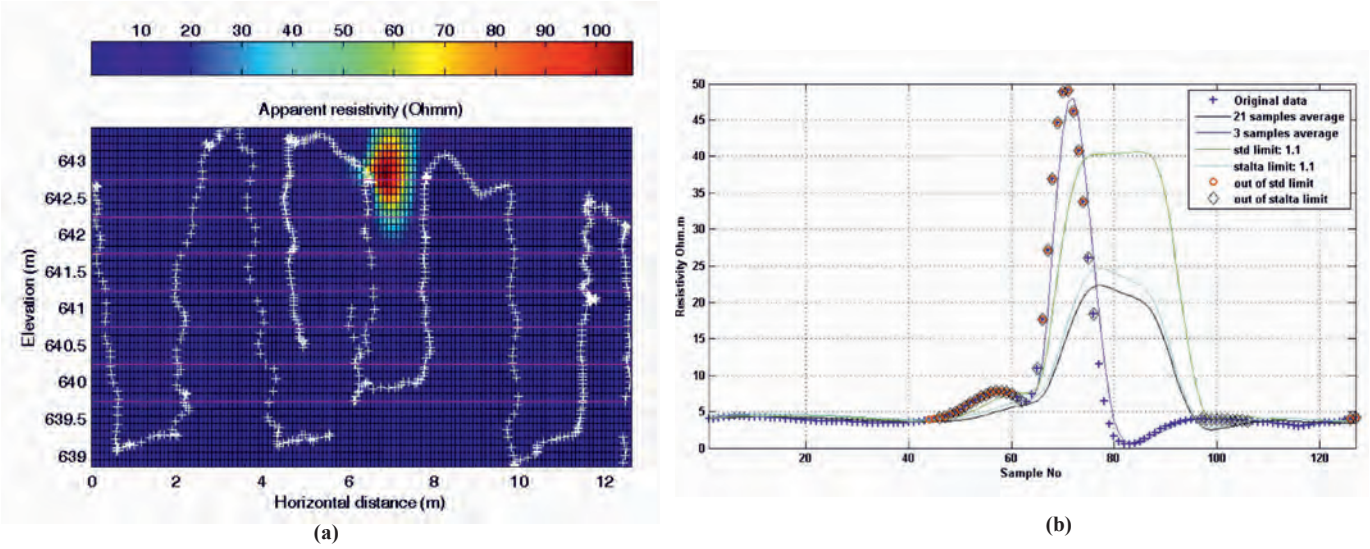

(a) (b)

Fig. 5. (Left) Apparent resistivity map deduced from experimental data acquired by the EM instrument CMD2. High resistivity values correspond to a hard rock inclusion occurrence. (Right) Results of SMHRD algorithm applied on the 4th cut showing the generated warning alerts at the positions where steep increase of resistivity values is encountered

Rys. 5. (Po lewej) Mapa rezystywności pozornej opracowana na podstawie danych eksperymentalnych uzyskanych przez instrument EM CMD2. Wysokie wartości rezystywności odpowiadają wystąpieniu wtrącenia skalnego. (Po prawej) Wyniki algorytmu SMHRD zastosowane podczas wybierania ostatniego pasma, pokazujące wygenerowane ostrzeżenia w miejscach, w których napotkano gwałtowny wzrost wartości rezystywności

open pit mine, Ptolemaida, Greece. Hard rock inclusions in form of layers and lenses lied within the clays. The map is the product of interpolation from apparent resistivity values acquired from the EM instrument CMD2 along the route marked with white crosses. High resistivity values correspond to an area where hard rock inclusion was observed. Separated data were extracted along 7 resistivity profiles with 0.5 m spacing and then data for five successive cuts (1-5) were derived to be used for processing. Figure 5 shows an example of Simple Mode Boulder Detection application along the 4th cut of the above mentioned experimental data. It shows an area marked with warning alerts (both out of standard deviation and STA/LTA limits), at the positions where steep increase of resistivity values is encountered.

Advanced Mode operation algorithms

Advanced Mode operation of the automated algorithm for real-time data evaluation requires the obtained data to be organized in profiles, resulting from the slewing operation of the bucket wheel. Since CMD2 instrument is mounted next to the bucket wheel at a certain distance (approximately 4 m), its trajectory is cyclic as it follows the movement of the bucket wheel. To calculate the coordinates (X, Y, Z) of the individuals trajectories of CMD2 corresponding to slewing operation of the bucket wheel we have modeled the excavation of a block by a BWE (Figure 6) when terrace cutting is applied. Figure 6 shows the X, Y and elevation coordinates from CMD2 synthetic instrument trajectories. Synthetic apparent resistivity

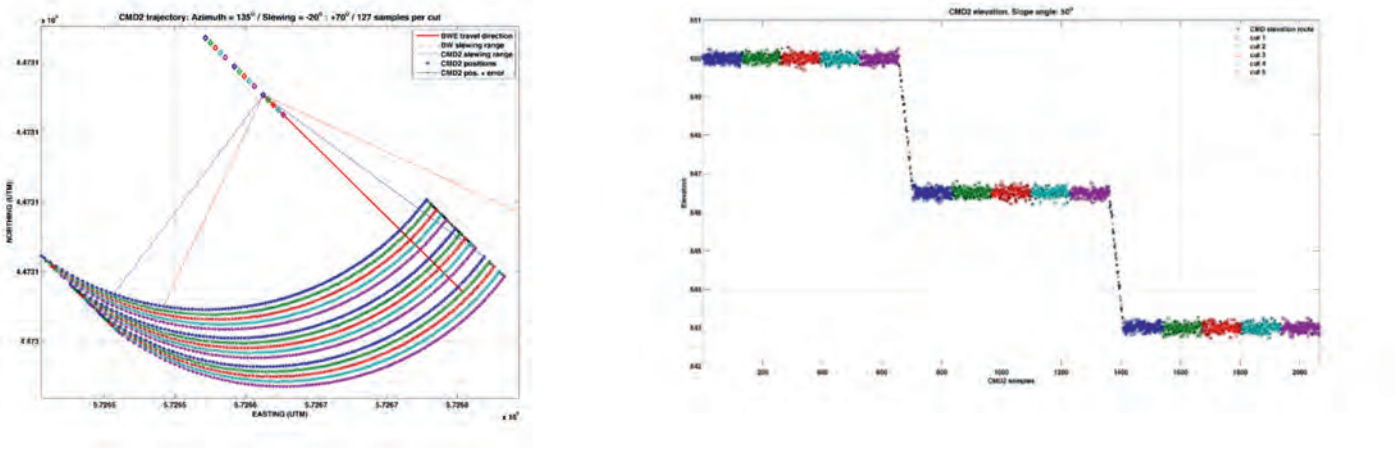

(a)

Fig. 6. (a) EM sensor (CMD2) trajectories in X-Y coordinates (UTM) during the excavation of a block by terrace cutting. (b) EM sensor (CMD2) elevations during the excavation of a block by terrace cutting

Rys. 6. (a) Trajektorie czujnika EM (CMD2) we współrzędnych X-Y (UTM) podczas wybierania kolejnych pasm w poszczególnych stopniach zabierki (b) Położenie czujnika EM (CMD2) podczas wybierania kolejnych pasm w poszczególnych stopniach zabierki

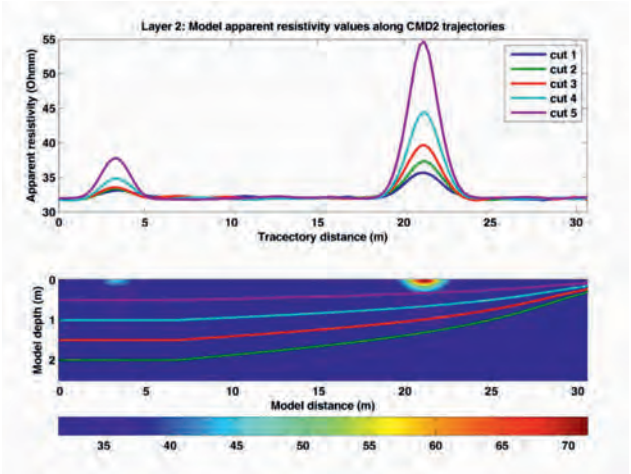

Fig. 7. Synthetic apparent resistivity data created along orthogonal models

Rys. 7. Dane syntetyczne dotyczące rezystywności pozornej utworzone za pomocą modeli ortogonalnych.

data created along orthogonal synthetic models were registered along the modeled bucket wheel trajectories (Figure 7). Subsequently, taking into account the above mentioned excavation process we organized the synthetic data in blocks, layers and cuts in order to form the resistivity profiles which are essential in Advanced Mode operation.

Hard rock inclusions increase the apparent resistivity within the EM profiles. Thus, local maxima detection is required in order to locate possible hard rock inclusions within the surrounding media. Within the Advanced Mode operation we have utilized two different algorithms for the detection of the hard rock formations which are described below.

Position Prominence Index

We utilize an algorithm for the detection of the most prominent peaks. Initially, we know that peaks define a subset of the local maxima, since several local maxima may be closely located and the values in between do not change dramatically. In such case, only the higher local maximum is considered as peak. The algorithm is very simple and exhibits the above mentioned qualitative description. It is adaptive regarding the number of required prominent peaks. The first peak is the global maximum. The next ones are recursively obtained from the immediately previous one. For each local maximum, the path to the previous peak is traced on the data. The prominence of a local maximum is the difference between the maximum value and the minimum value along the path. The next prominent peak is the one that is characterized by the maximum prominence. It is clear that this algorithm will return maxima with lower prominence values, as the number of required peaks increases. In practice this algorithm seems to agree with the subjective picking without increasing the complexity by adding extra parameters.

Since the excavation using a bucket-wheel excavator (BWE) is a repeated process along profiles, the high resistivity values caused by hard rock inclusions are anticipated: 1) at the same locations along profiles from the same front and 2) to be increased as the EM instrument (attached to BW) approaches the inclusion. The Position Prominence Index (PPI) is introduced to take into account the above mentioned criteria. Namely, the PPI value is increased in a specific position when resistivity peaks are detected repetitively and their values are increasing. The PPI of a current BWE pass is defined at positions of local resistivity maxima and depends on the value of the peak, the Number of Local Maxima along a pass and the proximity of the prominent peak in successive passes. If PR is the Prominence Rank, which depends on the value of the peak, and NLM the Number of Local Maxima met along this pass. Then, PPI is defined as:

$$PPI = \frac{NLM}{PR} \qquad (2)$$

The current PPI_{n+1} is subjected to modifications (bonus or punishments) according to:

a) $PPI_{n+1} = (PPI_n + PPI_{n+1})^2 - PPI_n$ when local resistivity maxima from successive BW passes are observed at the same position or $PPI_{n+1} = sqrt(PPI_n + PPI_{n+1})$ when local resistivity maxima from successive BW passes are observed at neighboring positions

b) $PPI_{n+1} = PPI_{n+1} * RES_{n+1} / RES_n$ for increasing or decreasing resistivity values at maxima from successive BW passes

PPI_n (B-W pass n) decreases according to:

a) $PPI_n = PPI_n / 2$

if PPI_{n+1} (BW pass n+1) < average(PPI_{n+1}) + 1 x standard_deviation(PPI_{n+1}), namely the current PPI_{n+1} value is not among the higher values

b) $PPI_n = PPI_n / 4$

if PPI_{n+1} (BW pass n+1) ≤ average(PPI_{n+1}), namely the

current PPI_{n+1} value is below current average PPI values.

Additional adjustments are:

- PPI_n is set to zero at positions where PPI_{n+1} is zero
- Following the previous adjustment, PPI of pass n+1 is updated to:

$PPI_{n+1} = PPI_n + PPI_{n+1}$

for the next iteration where data from the pass n+2 is involved.

PPI is an excellent position boulder detector technique. However, it suffers from two main drawbacks: a) it is sensitive to measurement position errors and b) there are difficulties in establishing PPI threshold, since PPI is affected by the number of data points in profiles. However, it is anticipated to contribute positively in the expert system, by increasing the success rate of hard inclusion detection.

A model of a conductive half space containing two non-conductive bodies was created and the apparent resistivity values corresponding to coil separation of 1.89 m are shown in Figure 8. Random noise equal to the 10% of half-space resistivity (32 Ohmm) was added to the model resistivity values. The resistive bodies are successively placed at shallower positions simulating the excavation of 0.5 m overburden at each pass of the B-W excavator. For the estimation of the PPI profile, we examine synthetic apparent resistivities. PPI values increase as the excavation front approaches the resistive bodies and thus, the geophysical instrument and the B-W excavator come closer to them. The highest PPI values are observed in Figure 8 at the positions x=5.5 m and x=22 m, where the centre of resistive bodies are located. The PPI values at the rest positions are suppressed due to the randomness of the apparent resistivity noise

Automatic evaluation of EM profiles based on Artificial Neural Networks for Pattern Recognition

The developed neural network model (Neural Network for Resistivity Pattern Recognition or NNRPR) is a feedforward *NN* with a hidden layer with 10 neurons that uses resistivity and positioning data from *n* successive cuts to estimate the probability of occurrence of a hard rock formation in the next cut (n+1) at a specific position x_o, y_o, z_o, as shown in Figure 9. The prediction is based on the examination of local changes of resistivity profiles created by the EM sensor (CMD2) mounted on the bucket-wheel during the excavation process. In terrace cutting, (Fig. 9), as bucket wheel is approaching the hard rock formations, the resistivity values are increasing due to the presence of the hard rock formation. These patterns of resistivity profiles indicate the presence of a hard rock formation as shown in Figure 9. The developed neural network model NNRPR is capable, after training, to recognize these patterns (changes in the resistivity profiles) and to relate them with the position of the hard rock formation.

NNRPR examines local changes of the resistivity profiles of the n recent successive cuttings by using a moving window including k resistivity measurements from each cut. In addition, NNRPR uses as input the distance among the examined successive local resistivity profiles. This distance coincides with the cutting advance of the BWE at the position x_o, y_o, z_o. Thus, the number of the inputs of NNRPR is $kxn+1$, while the output of NNRPR is the probability of the occurrence of a hard rock formation at position x_o, y_o, z_o. Several different values of n and k were examined during training and testing of NNRPR and optimal values were determined to be, n=3 and k=5.

NNRPR was trained by using a large set of synthetic data (178200 cases). Synthetic data simulate various geological and mining conditions which cannot be observed in a specific mine during a certain time period. With synthetic data hard rock formations of different size, shape, number and position can be effectively represented by creating the respective digital models. The random variations occurring in real data were taken into account by adding noise to synthetic data.

Synthetic data were then randomly divided into three sets: the training (70% of the original data), the validation (15%) and the testing (15%) set. Validation data were used to validate that

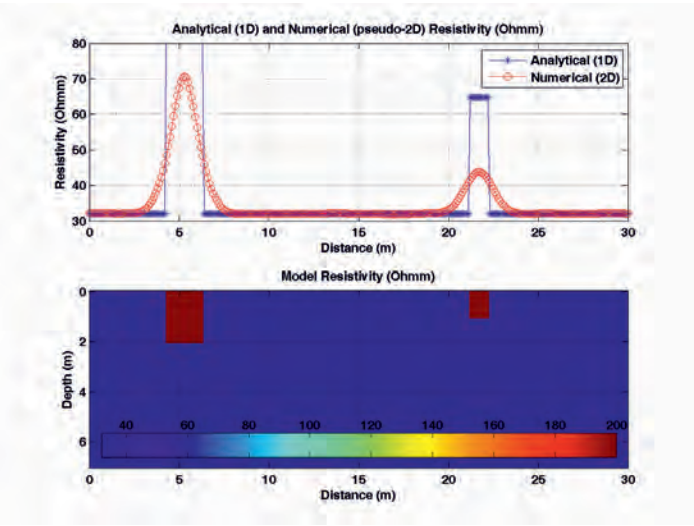

(a)

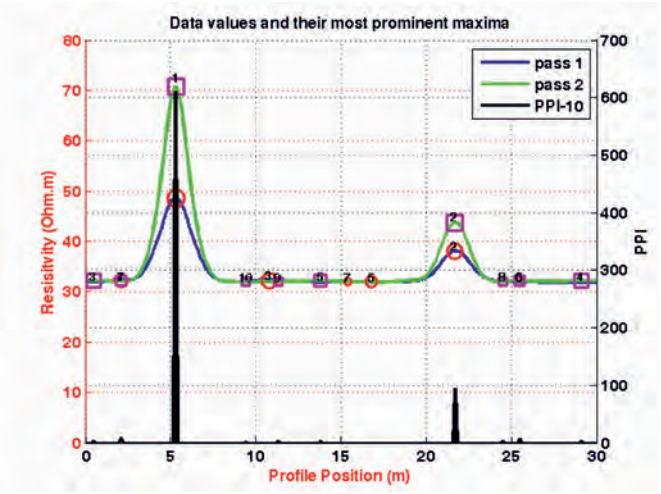

(b)

Fig. 8. (a) The apparent resistivity values as estimated by numerical approach over a 30 m x 7 m model. Two resistive (200 Ohmm) bodies are located at the surface (top of the bodies) within a homogeneous conductive (32 Ohmm) half space. (b) Apparent resistivity profiles corresponding to the fourth and fifth passes of B-W. Prominent maxima are detected in data profile positions x=5.5 m and x=22 m and thus, PPI (black line) is high there after five passes

Rys. 8. (a) Wartości pozornej rezystywności oszacowane metodą numeryczną w modelu 30 m x 7 m. Dwa ciała rezystancyjne (200 Ohmm) znajdują się na powierzchni o jednorodnej przewodności (32 Ohmm). (b) Widoczne profile rezystywności odpowiadają czwartemu i piątemu wybieranemu pasmu. Wyróżniające się maksima są wykrywane w pozycjach profilu danych x = 5,5 m i x = 22 m, wartość PPI (czarna linia) jest bardzo wysoka po wybraniu piątego pasma w analizowanym stopniu zabierki

the network is generalizing and to stop training before overfitting (early stopping technique), while testing data were used as a completely independent test of network generalization.

The development, training and testing of NNRPR was performed within the Matlab programming environment. The confusion matrix obtained after NNRPR training is shown in Figure 10. It shows the number and the percentages of correct and false predictions, where class 1 symbolizes the occurrence of hard rock formation while class 0 symbolizes the nonexistence. These percentages are considered acceptable. Figure 10 shows the obtained Receiver-Operator-Curve (ROC) as well, which indicates how the false alarms rate changes as the rate of successful prediction increases. From ROC it is obvious that the achievement of higher successful prediction rate (e.g. 0.98)

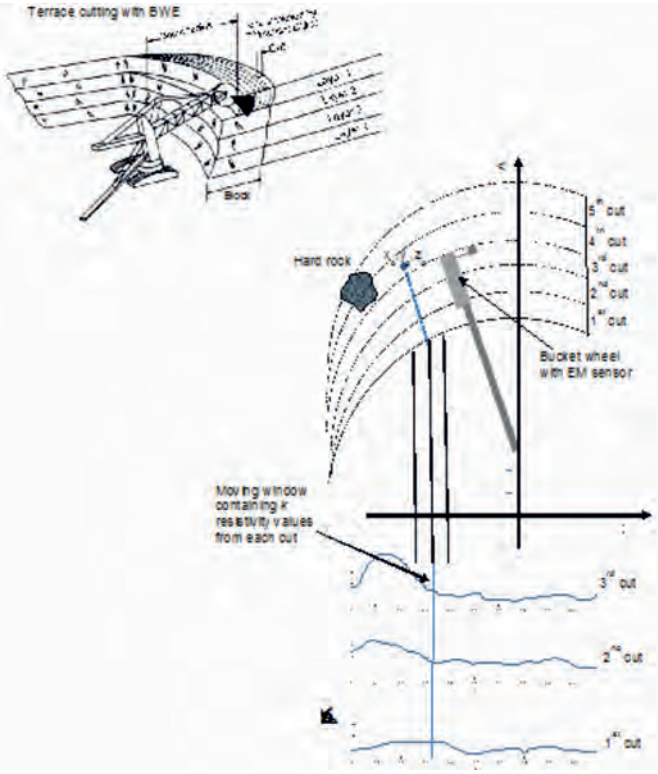

Fig. 9. Schematic diagram showing: (Top) Terrace cutting by BWE. (Bottom) Successive resistivity profiles obtained during terrace cutting (3 cuts) and use of moving window to examine local changes in resistivity profiles as BW approaches the hard rock

Rys. 9. Schemat przedstawiający: (Górny) Wybieranie pasm w poszczególnych stopniach zabierki. (Dół) Kolejne profile rezystywności uzyskane podczas wybieranych kolejno pasm (3 pasma) i wykorzystanie „ruchomego okna" do badania lokalnych zmian w profilach rezystywności, gdy koło urabiające zbliża się do nieurabialnej skały

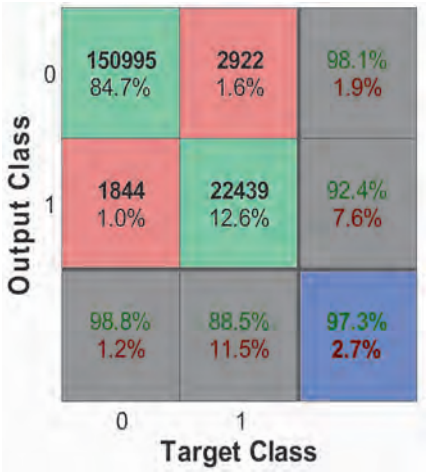

A

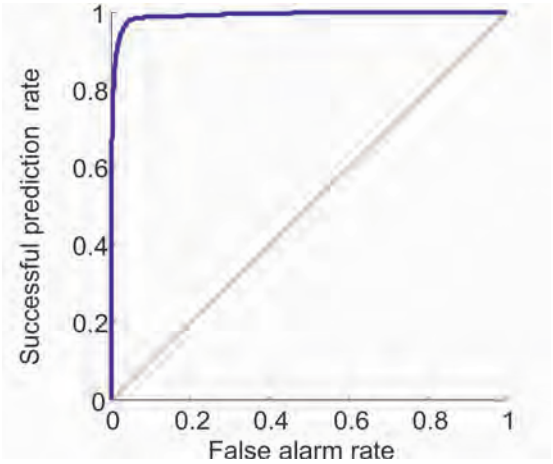

B

Fig. 10. (A) Confusion matrices for all data showing the number and the percentages of correct and false predictions (Class 0=Non-existence of a hard rock formation, Class 1=Existence of a hard rock formation). (B) The Receiver-Operator-Curve, or ROC, indicates how the false alarms rate increases as the rate of successful prediction increases

Rys. 10. (A Macierze pomyłek dla wszystkich danych z wyszczególnieniem liczb i wartości procentowych prognoz poprawnych i fałszywych (Klasa 0 = Brak istnienia twardej skały, Klasa 1 = Występowanie twardej skały). (B) Krzywa ROC wskazuje, w jaki sposób wzrasta liczba fałszywych alarmów wraz ze wzrastem wskaźnika pomyślnej prognozy

The trained NNRPR was then used to predict the occurrence of hard rock formations in real data collected with EM sensor (CMD2). These data was collected at the mine face of sector 7 of the South Field Mine of PPC. In the upper middle part of the mine face a hard rock formation was observed. The measurement points, as well as, the constructed resistivity map are shown earlier in Figure 5. The presence of the hard rock formation is clearly shown by the high resistivity values. Seven resistivity profiles with 0.5m spacing were created and then data for five successive cuts (1-5) were derived to be used as input to NNRPR to predict the probability of the occurrence of the hard rock formation. Predicted probabilities for each cut are shown in Figure 11. NNRPR has predicted the probability for a hard rock occurrence at cut 5 at the horizontal position of 7 m to the value of 0.92. For the other cuts (1-4) the predicted probability was very low (nearly zero).

CONCLUSIONS

We developed algorithms for automatic processing of data obtained from the geophysical sensor (electromagnetic conductivity-CMD2) and positioning system. First the overall system for data collection, pre-processing and evaluation was designed (block diagram). Subsequently, existing evaluation methods and algorithms were examined and the creation of the synthetic data required for the first phase of the development was completed.

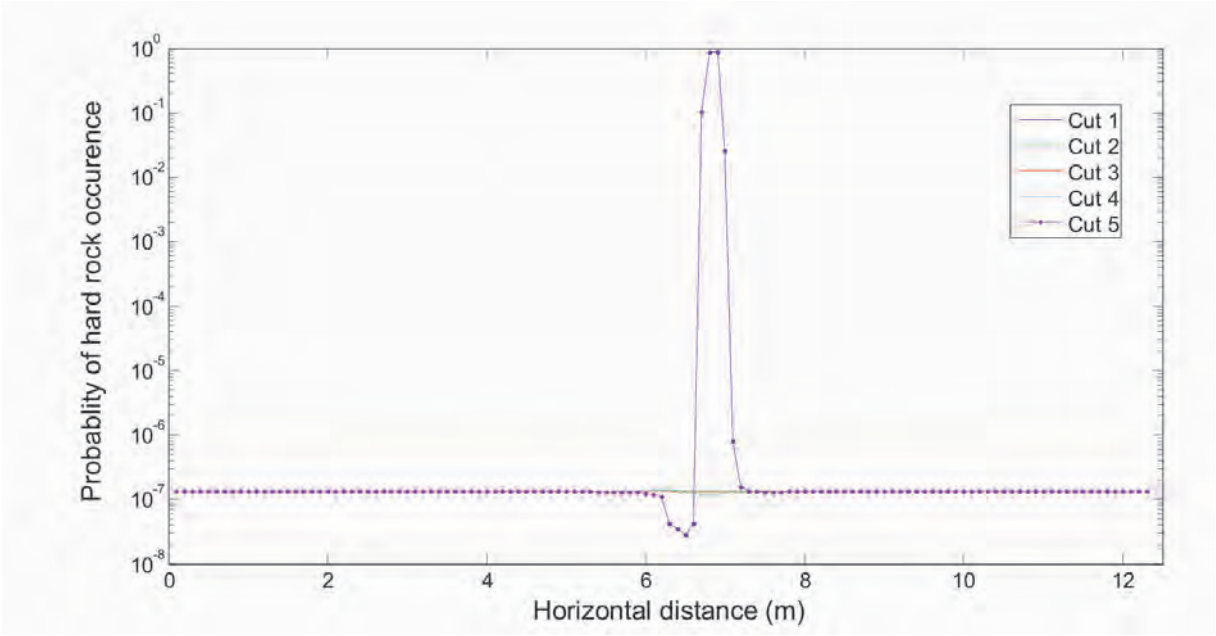

Fig. 11. Profiles of the probability for a hard rock occurrence for the examined five successive cuts (1-5)
Rys. 11. Profile prawdopodobieństwa wystąpienia twardej skały podczas wybierania kolejnych pasm w stopniu zabierki (1-5)

Several numerical, statistical and neural network models were created and tested with synthetic data as well as with data collected from the field test carried out in the coal-mines. Two different evaluation approaches were investigated, a relative simple one (Simple Mode) based on statistical process control and a more sophisticated one (Advanced Mode), based on PPI (Position Prominence Index) and on NNPR (Neural-Network based Pattern Recognition). The respective algorithms (software) were developed within Matlab programming environment. Both methods (simple and advanced) were tested extensively first with synthetic data and then with real data, collected using bucket truck as well as, with the EM sensor mounted on the bucket wheel of an excavator. Both in synthetic and real data, Advanced Mode provided more accurate results than Simple one in automatic detection of unmineable hard rock inclusions. However Advanced Mode algorithms are sensitive in positioning accuracy and require EM data from at least three successive cuts of the bucket wheel excavator sorted adequately. These requirements limit the use of Advanced Mode algorithms in real-time applications.

ACKNOWLEDGEMENTS

The research leading to these results has received funding from the European Commission - Research Fund for Coal and Steel under grant agreement No RFCR-CT-2015-00003. The presented results reflect only the authors' view and the European Commission is not liable for any use that may be made of the information contained therein.

Literature

[1] Galetakis M., Michalakopoulos T., Bajcar A., Roumpos C., Lazar M., Svoboda P. *Bucket wheel excavators operating under difficult mining conditions including unmineable inclusions and geological structures with excessive mining resistance,* Proced. of 13th International Symposium 'Continuous Surface Mining', 11-14 September 2016, Belgrade, 103-113

[2] Huss W., *Problems of Bucket-Wheel Excavators Body in Hardly-Workable Grounds in Polish Open Pit Mines*, C. Niemann-Delius. (ed.), Proc. of the 12th Int. Symp Continuous Surface Mining - Aachen 2014, Lecture Notes in Production Engineering, 59-71

[3] Kavouridis K., Roumpos C., Galetakis M. & Pavloudakis F. *Methods and Technological Improvements for the Efficient Removal of the Overburden Hard Rock Formations at South Field Lignite Mine*, Ptolemais, Greece, Proced.of 9th International Symposium 'Continuous Surface Mining', 8-11 October 2008, Petrosani – Romania, 91-100.

[4] McNeill, J.D., Electrical *Conductivity of Soils and Rocks*. Technical Note TN-5, Geonics, Ltd, 1980

[5] Nan M., Kovacs I., Andras I., Jula D., *Study of the working regime of the bucket wheel excavators in the conditions of Romanian open pit lignite mines*. 8th WSEAS International Conference on Simulation, Modelling and Optimization (SMO ,08) Santander, Cantabria, September 23-25, 2008, Spain

[6] Overmeyer L., Kesting M., and Jansen K., SIMT Technology – *Sensory identification of material type and detection of the interfaces*, Bulk Solids Handling, 2007, 27(2), 112-118